Cannabinoid receptor interacting protein 1a interacts with myristoylated $G\alpha_i$ N terminus *via* a unique gapped β-barrel structure

Received for publication, May 6, 2021, and in revised form, August 11, 2021 Published, Papers in Press, August 19, 2021,
https://doi.org/10.1016/j.jbc.2021.101099

William T. Booth[1], Jill E. Clodfelter[1], Sandra Leone-Kabler[2], Erin K. Hughes[1,2], Khalil Eldeeb[2], Allyn C. Howlett[2,3,*], and W. Todd Lowther[1,3,*]

From the [1]Department of Biochemistry and Center for Structural Biology, [2]Department of Physiology and Pharmacology and Center for Research on Substance Use and Addiction, Wake Forest School of Medicine, Winston-Salem, North Carolina, USA; [3]Center for Molecular Signaling, Wake Forest University, Winston-Salem, North Carolina, USA

Edited by Wolfgang Peti

Cannabinoid receptor interacting protein 1a (CRIP1a) modulates CB_1 cannabinoid receptor G-protein coupling in part by altering the selectivity for $G\alpha_i$ subtype activation, but the molecular basis for this function of CRIP1a is not known. We report herein the first structure of CRIP1a at a resolution of 1.55 Å. CRIP1a exhibits a 10-stranded and antiparallel β-barrel with an interior comprised of conserved hydrophobic residues and loops at the bottom and a short helical cap at the top to exclude solvent. The β-barrel has a gap between strands β8 and β10, which deviates from β-sandwich fatty acid–binding proteins that carry endocannabinoid compounds and the Rho-guanine nucleotide dissociation inhibitor predicted by computational threading algorithms. The structural homology search program DALI identified CRIP1a as homologous to a family of lipidated-protein carriers that includes phosphodiesterase 6 delta subunit and Unc119. Comparison with these proteins suggests that CRIP1a may carry two possible types of cargo: either (i) like phosphodiesterase 6 delta subunit, cargo with a farnesyl moiety that enters from the top of the β-barrel to occupy the hydrophobic interior or (ii) like Unc119, cargo with a palmitoyl or a myristoyl moiety that enters from the side where the missing β-strand creates an opening to the hydrophobic pocket. Fluorescence polarization analysis demonstrated CRIP1a binding of an N-terminally myristoylated 9-mer peptide mimicking the $G\alpha_i$ N terminus. However, CRIP1a could not bind the nonmyristolyated $G\alpha_i$ peptide or cargo of homologs. Thus, binding of CRIP1a to Gαi proteins represents a novel mechanism to regulate cell signaling initiated by the CB_1 receptor.

The CB_1 and CB_2 cannabinoid receptors are G protein–coupled receptors that are stimulated by endogenous eicosanoid agonists 2-arachidoylglycerol and anandamide as well as the phytocannabinoid Δ^9-tetrahydrocannabinol and its synthetic analogs (*e.g.*, CP55940) (1, 2). The CB_1 receptor (CB_1R) activates predominantly the $G\alpha_{i/o}$ family, initiating a variety of signaling pathways in cells in the nervous system, as well as numerous other cell types in liver, skeletal and smooth muscle, bone, heart, and endocrine organs (3–5).

For $G\alpha_{i/o}$ signaling, the C terminus of the receptor modulates the functional interactions (6). Nie and Lewis (7) determined that deletion of the CB_1R C-terminal (residues 418–472) released an inhibition of N-type Ca^{2+} channels in neurons, concluding that the C terminus performed an autoinhibition function and postulating that this might be due to an inhibitory protein that associates with the C terminus. A yeast two-hybrid screen using the human CB_1R C-terminal sequence as bait identified the cannabinoid receptor interacting protein 1b (CRIP1b) (expressed in primates), a splice variant of the predominant CRIP1a expressed in all vertebrate species (8). Exogenously expressed CRIP1a reversed CB_1R-mediated inhibition of Ca^{2+} channels in neuronal cells, whereas CRIP1b was not active (8). Subsequent studies demonstrated that CRIP1a expression compromised G protein coupling to CB_1R (9) and reduced the selectivity for $G\alpha_{i3}$ and $G\alpha_o$ (10).

The molecular mechanism by which CRIP1a modulates signaling has not been elucidated, and the lack of sequence similarity with other proteins has stymied the classification of function (11). We now report the crystal structure of CRIP1a, which identifies CRIP1a as a homolog to a family of cargo carriers for lipidated proteins and predicts a novel biochemical mechanism by which CRIP1a could function in cellular signaling.

Results and discussion

Crystal structure of CRIP1a reveals antiparallel β-barrel with a gap closed by a hydrogen-bonding network

To obtain structural clues for how CRIP1a interacts with CB_1R, rat CRIP1a was heterologously expressed in *Escherichia coli*. Unfortunately, the protein with or without the N-terminal His tag failed to crystallize. To solve this problem, protein

* For correspondence: W. Todd Lowther, tlowther@wakehealth.edu; Allyn C. Howlett, ahowlett@wakehealth.edu.
Present address for Khalil Eldeeb: Campbell University School of Osteopathic Medicine, Lillington, North Carolina 27546, USA, and Al Azhar Faculty of Medicine, Al Azhar University, New Damietta, Egypt.
Present address for William T. Booth: Johnson C. Smith University, Charlotte, North Carolina 28216, USA.

domains known to facilitate crystallization were appended to the N terminus and C terminus of CRIP1a (Fig. 1*A*), a strategy often used to crystallize G protein–coupled receptors and other transmembrane proteins (12). The T4 lysozyme (T4L) and thermostabilized apocytochrome b_{562}RIL (BRIL) tags were chosen as their molecular weight was only slightly larger than CRIP1a. The T4L protein contained the following site-directed changes to inactivate the enzyme (E11Q and D20N) and to remove Cys residues (C54T and C97A) to prevent thiol crosslinking (13, 14).

The best crystals were obtained for the T4L–CRIP1a protein. The structure (Table 1) was determined to 1.55 Å using the molecular replacement-single wavelength anomalous dispersion approach (15). The placement of the T4L molecule resulted in unambiguous electron density maps and enabled the positions of anomalous scattering for all possible sulfur sites in both proteins (Fig. 1*B*) to be determined. The resulting electron density maps allowed the building and refinement of the CRIP1a molecule and the linker between the protein domains. An examination of the crystal packing illustrates that the T4L domain facilitated packing within the lattice by surrounding the CRIP1a molecule (Fig. 1*C*). The final model of T4L–CRIP1a was 82.9% complete with reasonable geometry (Table 1). Most of the missing residues were within T4L domain, which will not be considered further.

CRIP1a contained a 10-stranded, antiparallel β-barrel with a prominent gap between strands β8 and β10 (Fig. 1*D*). The interior of the β-barrel was lined with conserved hydrophobic residues (Fig. 1*E* and alignment in Fig. S2). The gap in the β-barrel was held together by a hydrogen-bonding interaction between Trp121 and Tyr145 and a hydrogen-bonding network that includes Thr119 and Glu161 and water molecules (Fig. 1*E*). Solvent is excluded from the bottom and top of the barrel by loops and a short helical cap, respectively. For the latter, Val23, Ile38, and Leu40 were packed against the Tyr46, Tyr89, and Trp121 at the top of the hydrophobic core, thereby excluding aqueous solvent from the barrel interior.

CRIP1a contrasts with CRIP1b and previous computational models

With the new structure in hand, CRIP1a was compared with its isoform CRIP1b, a previous core domain proposal, and two computational models that proposed Rho-guanine nucleotide dissociation inhibitor (GDI) as a homolog. The following paragraphs discuss these topics in turn.

The sequence of CRIP1b does not contain residues 125 to 164 of CRIP1a (*yellow* in Fig. 2*A*) and would result in the loss of strands β9 and β10 and the entire cap structure. In one previous study, the systematic deletion of N-terminal and C-terminal sequences revealed that residues 34 to 110 (Fig. 2*B*) could interact with CB_1R in a yeast two-hybrid reporter assay (8). The loss of residues 1 to 33 and 111 to 164 would remove over half of the CRIP1a protein and the internal hydrophobic core. In both truncation scenarios, the resulting exposure of the hydrophobic core of the protein suggests that these forms may not be stable unless bound to another protein partner.

Two computational studies used a panel of algorithms to assign the secondary and tertiary structures of CRIP1a and CRIP1b (16, 17). Both studies identified the hematopoietic Rho-GDI2 (Rho-GDIβ or Ly/D4GDI) as the best threading result despite the low (15.9%) sequence identity. A superimposition of the CRIP1a crystal structure onto that of Rho-GDI2 (Fig. 2*D*) illustrates significant dissimilarity between the proteins (RMSD of 4.6 Å over 96 residues). Both studies (16, 17) calculated the binding mode of the last nine residues of the CB_1R C terminus onto the CRIP1a computational model. Mapping of the putative CRIP1a–CB_1R interface residues (Lys76, Arg82, Asn61, Tyr85, Lys124, and Lys130 for CRIP1a; Glu77, Asp79, Arg82, Tyr 85, Tyr89, Tyr 124, and Cys126 for CRIP1b) onto the CRIP1a structure (Fig. 2, *E* and *F*), however, illustrates that the proposed interaction surfaces were not contiguous.

Rho-GDIs are cytosolic proteins that exist in a 1:1 stoichiometric association with the small G protein Rho and function to preclude GDP dissociation from inactive Rho. Rho-GDIs also inhibit the hydrolysis of GTP by guanine-nucleotide exchange factors or GTPase-activating proteins (18). Rho-GDIs are β-sandwich proteins that contain a flexible N-terminal helix–loop–helix structure that interacts with the switch regions of the small G protein (19). It is unlikely that CRIP1a can serve a GDI function because CRIP1a lacks this regulatory domain. However, the C-terminal domain of Rho-GDI is an immunoglobulin-like β-sandwich comprised of nine β-strands in two antiparallel sheets. This structure forms a hydrophobic interior, which accommodates the isoprenyl group of small G proteins within its interior to serve a carrier function for cytosolic to membrane redistribution (19, 20). The C-terminal domain of Rho-GDI exhibits the greatest structural and perhaps functional homology with CRIP1a.

CRIP1a most likely does not function as a fatty acid–binding protein

Considering the endogenous ligands of the CB_1R, one could hypothesize that CRIP1a might function in a manner analogous to intracellular lipid carrier proteins (Fig. 2*F*) (21, 22). Fatty acid–binding proteins (FABPs) accommodate 2-arachi-do noylglycerol and anandamide (23, 24) as well as tetrahydrocannabinol and cannabidiol (25). The cellular retinal–binding protein-1 accommodates abnormal cannabidiol and fatty acids (22, 26). FABPs and cellular retinal–binding protein-1 are β-clamshell proteins configured as two orthogonal 5-stranded β-sheets capped by a helix–loop–helix motif. Endocannabinoid amide or glyceride moieties interact *via* hydrogen bonding, and the arachidonoyl moiety is configured in a U shape within FABP5 (24). Attempts to either form CRIP1a cocrystals or to soak crystals with stable endocannabinoid analogs and CP47497 failed to induce a structure that differed from the conformation depicted herein or to show electron density for ligands (data not

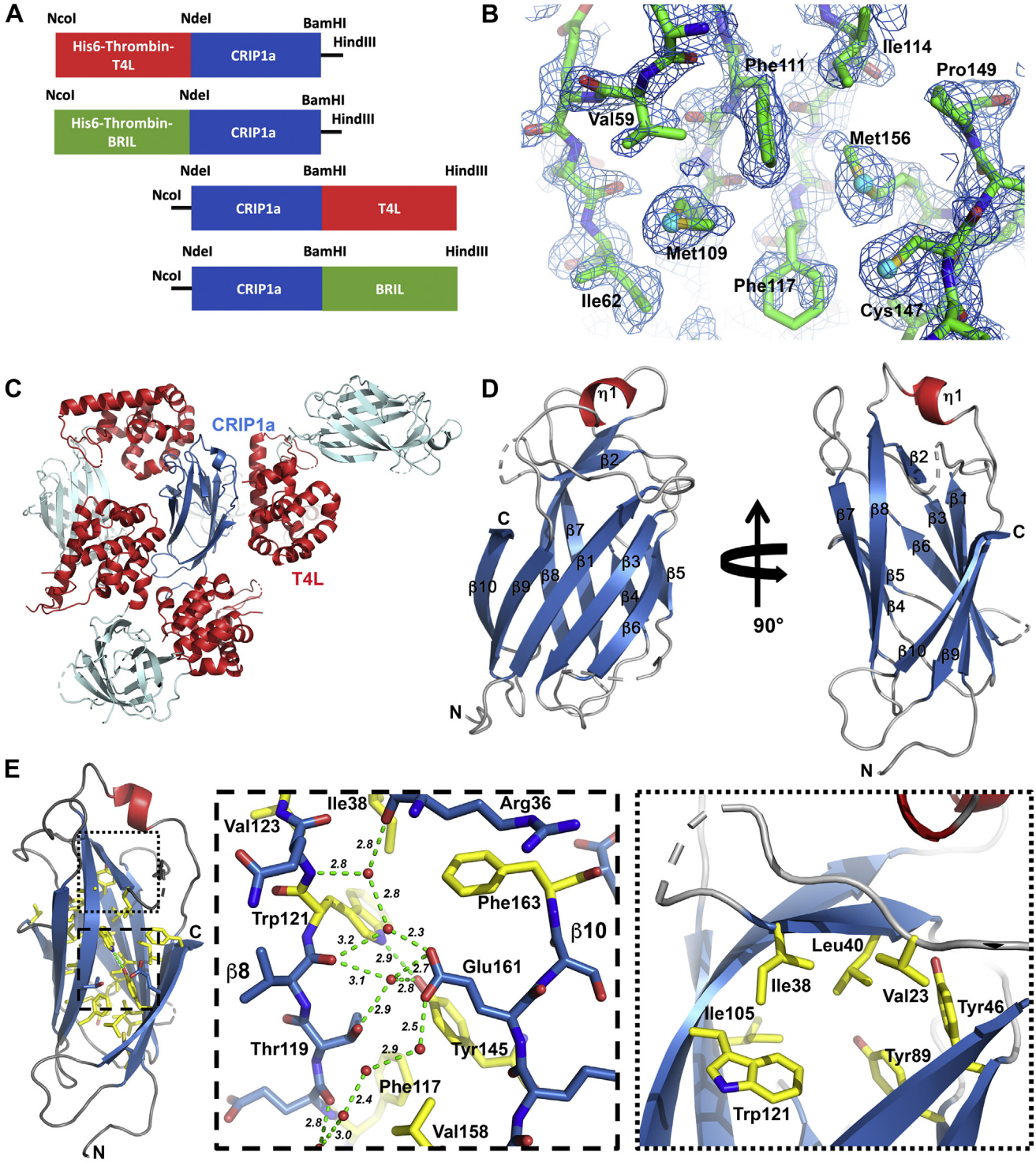

Figure 1. Structure of CRIP1a determined to a resolution of 1.55 Å. *A*, crystallization tag strategy for CRIP1a. *B*, representative 1.5 σ $2F_o$–F_c map within the hydrophobic core of CRIP1a. *Cyan blue spheres* indicate sulfur sites determined by single-wavelength anomalous dispersion (SAD). These sites superimpose with the sulfur atoms of the final model; see text for details. *C*, crystal packing illustrates that the T4L molecule helped to prevent CRIP1a–CRIP1a interactions. *D*, secondary structure of CRIP1a in two orthogonal views. Importantly, the antiparallel β-barrel is missing one β-strand between strands β8 and β10. *E*, key interactions of the hydrophobic core (*yellow*) near the β-strand gap and the "lid" of the barrel. A hydrogen-bonding network, involving Tyr145, Trp121, Thr119, Glu161, backbone atoms of the β8 strand, and water molecules, "stitches" the β-barrel closed (distances in Å indicated by *dashed green lines*). The lid of the barrel excludes solvent *via* the interaction of residues Val23, Ile38, Leu40, Tyr46, Tyr89, Ile105, and Trp121. CRIP1a, cannabinoid receptor interacting protein 1a; T4L, T4 lysozyme.

shown). Additional studies may be warranted in this area, but the next sections provide convincing evidence that CRIP1a binds a different type of cargo.

CRIP1a is structurally homologous to cargo carrying proteins

The DALI server (Biocenter Finland; http://ekhidna2.biocenter.helsinki.fi/dali/) was used to identify structural

Table 1
Data collection and refinement statistics

Structure	His-T4L–CRIP1a
Protein Data Bank code	6WSK
Wavelength (Å)	1.54
Resolution range (Å)	19.86–1.55 (1.61–1.55)[a]
Space group	P 41 21 2
Unit cell (Å, °)	68.2 68.2 146.6 90 90 90
Total reflections	1,021,550 (57,346)
Unique reflections	50,935 (4957)
Multiplicity	20.1 (11.6)
Completeness (%)	99.8 (99.3)
Mean I/σI	28.4 (2.0)
Wilson B-factor (Å^2)	21.1
R-merge	0.059 (1.25)
R-measure	0.060 (1.31)
R-pim	0.010 (0.37)
CC1/2	1 (0.75)
CC*	1 (0.93)
Reflections used in refinement	50,932 (4957)
Reflections used for *R*-free	1689 (164)
R-work	0.208 (0.261)[b]
R-free	0.225 (0.288)
Number of nonhydrogen atoms	2551
Macromolecules	2334
Solvent	217
Protein residues	287
RMS (bonds)	0.010
RMS (angles)	1.10
Ramachandran favored (%)	99.3
Ramachandran allowed (%)	0.7
Rotamer outliers (%)	0.0
MolProbity clash score	4.9
Average B-factor (Å^2)	36.4
Macromolecules	36.4
Solvent	36.7
Number of TLS groups	7

[a] Statistics for the highest-resolution shell are shown in parentheses.
[b] 17.1% of the structure was missing (59 of 346 residues) from the crystallization tag.

homologs of CRIP1a (27). Despite having <6% sequence identity, the β-sandwich hydrogen-bonding pattern matches to phosphodiesterase 6 delta subunit (PDE6δ) (also known as inositol polyphosphate-5-phosphatase) and Unc119 (28). PDE6δ functions as a solubilizing factor that binds C-terminally farnesylated Ras family small G proteins, facilitating their movement to the plasma membrane (29–31). In the PDE6δ–farnesylated-Rheb complex (Fig. 3*A*), the β-barrel opens to accept the prenyl moiety into the top of the hydrophobic core, a core like that seen in CRIP1a (Fig. 1*E*). Although Unc119 also has a hydrophobic core like CRIP1a and PDE6δ, Unc119 carries N-terminally myristoylated proteins to the membrane (32). Importantly, the N-myristoylated ciliopathy protein nephrocystin-3 cargo (Myr-NPHP3; Fig. 3*B*) enters the opening on the side of the β-sandwich but still places the myristoyl moiety into a hydrophobic binding pocket as seen for PDE6δ.

Since the CRIP1a structure exhibits structural homology with lipidated-protein cargo carriers, we hypothesize that CRIP1a exhibits functional homology to serve a shuttling or sequestrating function for lipidated proteins. CRIP1a may serve a function homologous to PDE6δ, leading to the predicted transport of C-terminally prenylated cargo entering near the helical cap (Fig. 3, *A* and *C*). Alternatively, a functional homology with Unc119 would predict that CRIP1a could accommodate medium-chain unsaturated fatty acids of N-terminally acylated proteins entering from the side in the opening afforded by the "missing β-strand" of the β-sandwich structure (depicted in Fig. 3, *B* and *C*).

CRIP1a can bind the N-terminally myristoylated Gα$_i$ peptide

To deduce what the cargo might be for CRIP1a, we evaluated two proteomics reports that describe proteins that appear in complexes with the CB$_1$R and identified several lipidated proteins, which include heteromeric G protein subunits (33, 34). We had previously observed that as the levels of CRIP1a were experimentally manipulated in neuronal cells, the Gα$_i$ protein subtypes that could be activated by CB$_1$R stimulation were changed (10). For example, increasing the protein expression of CRIP1a led to a reduction in agonist-stimulated CB$_1$R activation of Gα$_{i3}$, suggesting that CRIP1a might sequester this particular isoform.

To test that CRIP1a could bind Gα subunits through their N-terminal myristoyl moiety, we monitored the binding of the corresponding fluorescein-labeled peptide (Myr-GCTLSAEDK-5Flu) to CRIP1a using fluorescence polarization (Fig. 3*D*). It is important to note that the N-terminal sequences for these Gα isoforms (Gα$_{i1/2/3/o}$) are identical. The corresponding nonmyristoylated peptide was used as the control. With the structural homology to Unc119 and PDE6δ, we also tested their representative myristoylated and farnesylated cargo peptides (Myr-NPHP3, Myr-GTASSLVSPK-5Flu; Rheb-Farn, 5Flu-SQGKSSC(Farn)-OMe).

CRIP1a bound the Gα$_i$ peptide with a K_d of 21.2 ± 2.3 μM, a value consistent with myristoylated peptides of different sequences binding to Unc119 (0.05–200 μM) and farnesylated peptides binding to wildtype PDE6δ and site-directed variants (0.3–3 μM) (30, 32, 35). Importantly, CRIP1a was unable to readily bind the nonmyristoylated Gα peptide or the Myr-NHPH3 peptide. These data support that CRIP1a requires the Myr moiety and makes sequence-specific contacts with the peptide. The inability to bind the Rheb-Farn peptide supports that CRIP1a does not bind farnesylated cargo, consistent with the observation that lipidated cargo carrying proteins shuttle cargoes of only one lipid type.

Although these preliminary data are consistent with CRIP1a-binding myristoylated Gα$_i$ cargo, there are clear caveats to this facile interpretation. Peptide pull-down and yeast two-hybrid screen assays have demonstrated that the CB$_1$R distal C terminus binds to CRIP1a (8, 36). We also know that the CB$_1$R proximal C-terminal eighth helix functionally interacts with Gα$_{i3}$ (37). The recent crystal structures of CB$_1$R and the cryo-EM structure of the CB$_1$R–Gαβγ complex illustrate the relative proximity of each of the protein domains (38–41). While the C-terminal α8 helix of CB$_1$R is on the same side of the megacomplex as the N-terminal region of the Gα subunit, the distal C-terminal region of CB$_1$R known to interact with CRIP1a (residues 464–472) was not delineated (8). As such, one cannot predict at this time how CRIP1a could interact with both proteins at the same time. Thus, much work is needed to evaluate the role of the CB$_1$R C terminus and the temporal and spatial features of the CB$_1$R–CRIP1a–Gα protein interaction.

A sequence alignment of CRIP1a from rat, mouse, human, cow, frog, and fish (Fig. S2; 99%–59% sequence identity to rat CRIP1a, respectively) indicates that interfaces I1 (Farn cargo)

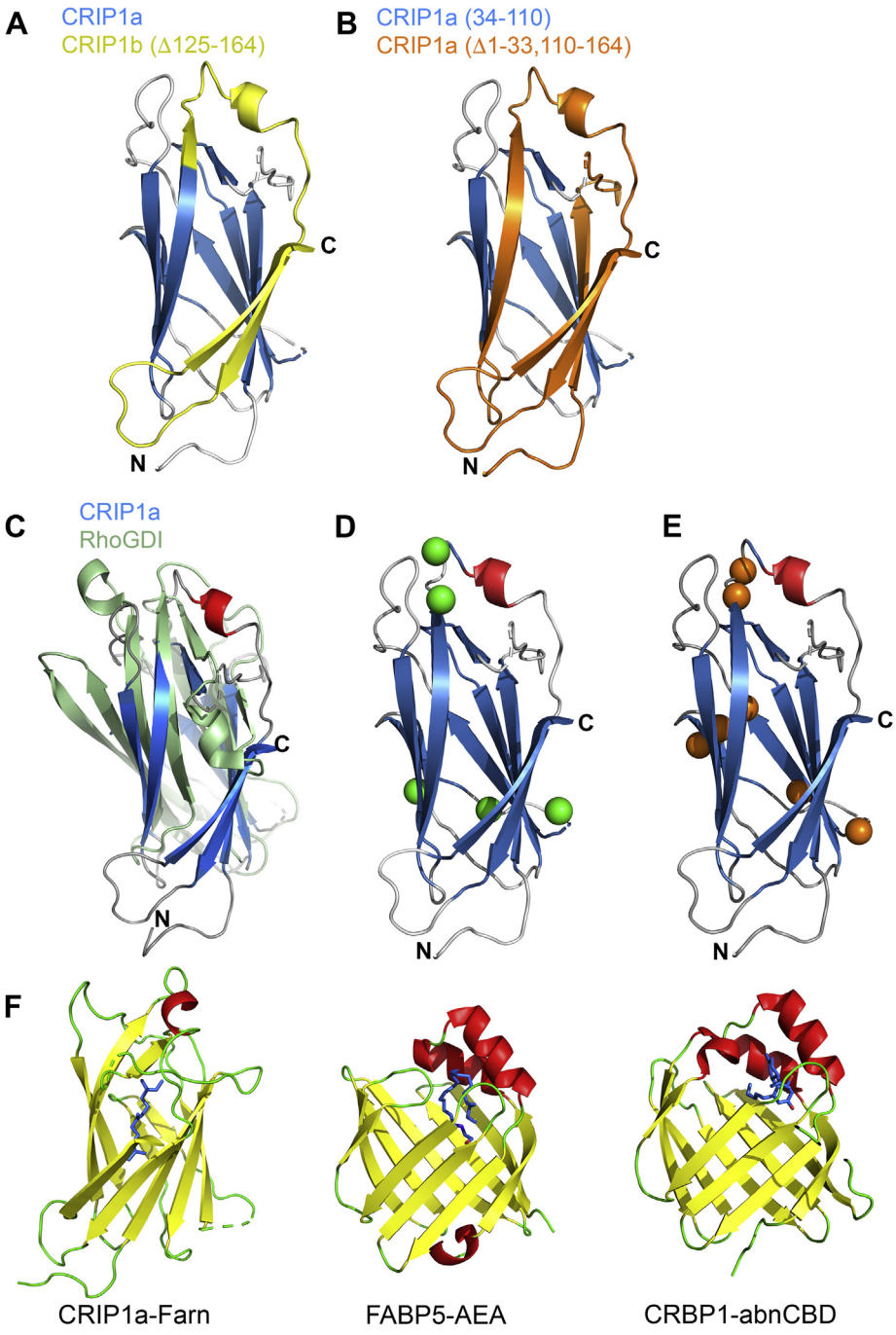

Figure 2. Comparison of CRIP1a variants and previous models derived *in silico*. *A*, comparison of CRIP1a *versus* CRIP1b. The transcript for CRIP1b prematurely truncates the protein at residue 125 (*blue*), with *yellow* showing truncated residues 126 to 164. *B*, comparison of full-length CRIP1a to the originally proposed functional "core" of CRIP1a (residues 34–110; *blue*); residues 1 to 33 and 111 to 164 would be truncated (*orange*) in this scenario. *C*, superposition of CRIP1a (*blue*) and Rho-GDI2 (Protein Data Bank [PDB] ID: 5H1D) (*green*) (47). *D* and *E*, location of residues proposed to interact with CB_1R C terminus: *D*, by Ahmed *et al.* (16) (*green spheres*) or *E*, by Singh *et al.* (17) (*orange spheres*). *F*, comparison of the secondary structure and lipid-binding regions of CRIP1a, FABP5, and CRBP1. Lipid moieties are colored *blue*. The farnesyl group is modeled into the CRIP1a internal cavity based on the PDE6δ complex, see Figure 3 and associated text. The ligand for human FABP5 is anandamide (AEA) (PDB ID: 4AZN) (24). The ligand for human CRBP1 is an "abnormal" cannabidiol (abn-CBD) identified by Silvaroli *et al.* (PDB ID: 6E5L) (26). CB1R, CB1 receptor; CRBP1, cellular retinal–binding protein-1; CRIP1a, cannabinoid receptor interacting protein 1a; CRIP1b, cannabinoid receptor interacting protein 1b; FABP5, fatty acid–binding protein 5; GDI2, guanine nucleotide dissociation inhibitor; PDE6δ, phosphodiesterase 6 delta subunit.

and I2 (Myr cargo) are the most conserved. Studies are underway to systematically test a broader pool of candidate myristoylated and farnesylated peptides and intact proteins using assays that have been validated for the PDE6δ and Unc119 proteins (28, 32).

Conclusions

The new structure of CRIP1a, its predicted protein interface surfaces and cargoes, and its ability to bind N-terminally myristoylated $G\alpha_i$ peptide support a new model with which to test hypotheses regarding function of the CRIP1a protein to

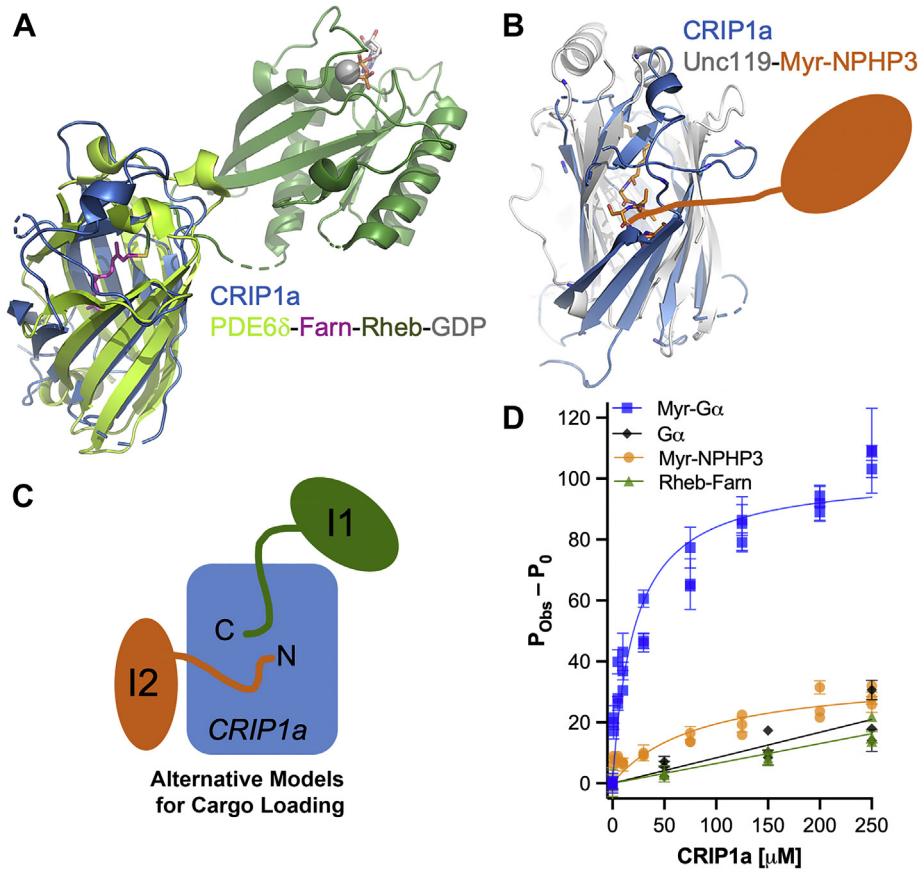

Figure 3. Comparison of CRIP1a to structural homologs and model for cargo interactions. *A*, CRIP1a (*blue*) superimposed onto PDE6δ bound to C-terminally farnesylated Rheb-GDP (Protein Data Bank ID: 3T5G; RMSD 4.0 Å over 96 residues) (35). For this panel and all others, the color key for each protein, lipid, and cofactor are indicated. *B*, CRIP1a superimposed onto UNC119 bound to the N-terminally myristoylated NPHP3 peptide (PDB ID: 5L7K; RMSD: 5.3 over 96 residues) (32). *C*, model for the protein interaction surfaces of CRIP1a. Interface 1: C-terminally farnesylated cargo. Interface 2: N-terminally myristoylated cargo. *D*, fluorescence polarization analysis of peptides binding to CRIP1a. See main text for peptide sequences. CRIP1a, cannabinoid receptor interacting protein 1a; PDE6δ, phosphodiesterase 6 delta subunit.

modify the signal transduction efficacy of the CB_1R (8–10) by modulating interactions with heterotrimeric G proteins (42).

Experimental procedures

Expression and purification of recombinant proteins

The genes for rat CRIP1a, T4L, and apocytochrome BRIL (43) were codon optimized for *E. coli* expression by GenScript. Expression plasmids were generated with either the T4L and BRIL genes cloned onto the N-terminal side (NcoI–NdeI sites) or the C-terminal side (BamHI–HindII sites) of CRIP1a within the pET28b vector (Fig. 1*A*). For the N-terminal T4L and BRIL crystallization tags, a noncleavable 6-His tag was also installed. The DNA sequence of all constructs was verified.

All proteins were expressed and purified using the following protocol. The expression vector was freshly transformed into C41(DE3) *E. coli* cells. The next morning, the plates were scraped, and a 1 l culture of LB broth with kanamycin (50 μg/ml) was grown for 2 h at 37 °C rotating at 200 rev/min. This culture was used to inoculate two 10 l cultures with pre-warmed LB broth within 11 l fermentation vessels. The cells were grown with aeration (10 l/min air, 200 rpm propeller speed) until an absorbance of 0.8 at 600 nm was reached. The temperature was then reduced to 16 °C. Once the lower temperature was reached, IPTG was added to 0.2 mM, and the cells were grown overnight. The resulting cell pellets were combined and stored at −80 °C. The typical yield from a preparation was 2 to 5 mg/l of culture.

The cell pellets were crushed to a powder and resuspended in 200 ml of +T/G buffer (20 mM Hepes, pH 7.9, 500 mM KCl, 5 mM imidazole, 1 mM $MgCl_2$, 10% glycerol, 0.1% Triton X-100, 0.1 mM phenylmethylsulfonyl fluoride, 0.1 mM benzamidine, and 5 mg DNase). The cells were lysed by three passages through an Avestin Emulsiflex C3 homogenizer operated at >15,000 psi. The lysate was clarified by centrifugation (45 min, 35,000*g*, twice) and filtered using a 0.45-μm filter before loading onto a pre-equilibrated HisPur Cobalt Superflow agarose column (Thermo Scientific), at a flow rate of 5.0 ml/min. CRIP1a was eluted from the column using a 5 to 250 mM imidazole gradient. The protein was further purified by S-sepharose ion exchange and Superdex 200 size-exclusion columns (Fig. S1). This last step exchanged the protein into its final storage buffer (20 mM Hepes, pH 8.0, 100 mM NaCl, and 0.1 mM EDTA). CRIP1a protein was concentrated, aliquoted, frozen with liquid N_2, and stored at −80 °C.

Crystallization and data collection

CRIP1a alone and the panel of T4L/BRIL fusions were screened for crystallization conditions using vapor diffusion experiments with a variety of commercial screens, 96-well Intelliplates (ARI), and a Crystal Gryphon (ARI) robot. Equal volumes of protein (0.2 μl; 15–30 mg/ml) and the well solution were mixed and incubated at 20 °C. Several crystallization hits were identified, optimized, and screened for their quality and extent of diffraction. The best crystals were for His6-T4L–CRIP1a. The final optimized crystals were grown in 24-well sitting plates using the following conditions: 30 mg/ml, 0.1 M sodium citrate (pH 4–5.5), and 0.3 to 0.6 ammonium sulfate. The crystals were placed in Paratone N (Hampton Research) as a cryoprotectant for data collection at 100 K. Diffraction data (0.25° oscillation images) was collected in house on a Rigaku 007/Dectris Pilatus 3R system and processed with CrysAlis (Pro) (version 3.49) (Rigaku) (Table 1).

Structure solution, refinement, and comparisons

All structure solution and refinement steps were performed using the PHENIX suite of programs and the molecular replacement-single wavelength anomalous dispersion method (15). The molecular replacement step used the T4L structure (Protein Data Bank ID: 3FA0) as a search model (44). With this solution in hand, PHASER was able to use the anomalous signal to locate all sulfur atoms within Met and Cys residues (12 total) of T4L and CRIP1a (FOM 0.42). The resulting 1.55 Å maps enabled AUTOBUILD to generate the first model. This starting model was iteratively modified and rebuilt with COOT, using the analysis from MOLPROBITY and omit maps as a guide (45, 46). The residues within the Protein Data Bank file correspond to the following: His6-T4L (residues −182 to −1) and CRIP1a (residues 1–164). The following residues were not visible in the electron density (59 of 346 residues or 17.1%): for T4L, residues −182 to −166, −145 to −141, −131 to −110; for CRIP1a, residues 27 to 35 and 76 to 81. Structural homologs of CRIP1a were identified using the DALI program (27). All structural figures and superpositions were generated with PyMOL (version 2.1) (Schrödinger, Inc).

Fluorescence polarization

Fluorescein-labeled peptides were synthesized and purified by Cambridge Peptides, Ltd. Recombinant CRIP1a (0–250 μM) was added to 20 nM peptide and incubated at room temperature for 30 min, in the final buffer (25 mM Hepes, pH 7.5, 100 mM NaCl, 5 mM $MgCl_2$, 0.1 mM EDTA, 2 mM Tris (2-carboxyethyl) phosphine hydrochloride, and 10% glycerol). Fluorescence polarization was monitored (λ_{ex} = 470 nm and λ_{em} = 530 nm) using an Infinite M1000 PRO plate reader (Tecan Instruments). New protein dilutions were tested on three separate days with a fresh peptide aliquot. Each concentration was tested as biological quadruplicates. For those peptides showing saturation, all data were plotted and globally fit to a single binding site model using PRISM 9.1 (GraphPad). Data are plotted as mean ± SEM.

Data availability

Data for all figures are contained within the article. The coordinates and structure factor files have been deposited to the Protein Data Bank with code 6WSK.

Supporting information—This article contains supporting information.

Acknowledgments—The authors thank the following individuals for their contributions to the project: Lynnette Johnson, Thomas Jönsson, Jenny Collins, Wayne Hemphill, and Brandon Travis.

Author contributions—W. T. B., A. C. H., and W. T. L. conceptualization; J. E. C., S. L.-K., and K. E. methodology; W. T. B., A. C. H., and W. T. L. validation; W. T. B., J. E. C., A. C. H., and W. T. L. formal analysis; W. T. B., J. E. C., S. L.-K., E. K. H., K. E., and W. T. L. investigation; W. T. B. data curation; W. T. B., J. E. C., A. C. H., and W. T. L. writing–original draft; W. T. B., J. E. C., S. L.-K., E. K. H., K. E., A. C. H., and W. T. L. writing–review and editing; A. C. H. and W. T. L. visualization; A. C. H. and W. T. L. supervision; A. C. H. and W. T. L. project administration; A. C. H. and W. T. L. funding acquisition.

Funding and additional information—Funding for this study was provided by National Institute on Drug Abuse R01-DA042157 to W. T. L. and A. C. H. W. T. B. was supported by the National Institute of General Medical Science, National Institutes of Health K12-GM102773. The content is solely the responsibility of the authors and does not necessarily represent the official views of the National Institutes of Health.

Conflict of interest—The authors declare that they have no conflicts of interest with the contents of this article.

Abbreviations—The abbreviations used are: BRIL, b_{562}RIL; CB_1R, CB_1 receptor; CRIP1a, cannabinoid receptor interacting protein 1a; FABP, fatty acid–binding protein; GDI, guanine nucleotide dissociation inhibitor; PDE6δ, phosphodiesterase 6 delta subunit; T4L, T4 lysozyme.

References

1. Lu, H. C., and Mackie, K. (2016) An introduction to the endogenous cannabinoid system. *Biol. Psychiatry* **79**, 516–525
2. Mechoulam, R., Hanus, L. O., Pertwee, R., and Howlett, A. C. (2014) Early phytocannabinoid chemistry to endocannabinoids and beyond. *Nat. Rev. Neurosci.* **15**, 757–764
3. Turu, G., and Hunyady, L. (2010) Signal transduction of the CB_1 cannabinoid receptor. *J. Mol. Endocrinol.* **44**, 75–85
4. Howlett, A. C., and Abood, M. E. (2017) CB_1 and CB_2 receptor pharmacology. *Adv. Pharmacol.* **80**, 169–206
5. Oliver, E. E., Hughes, E. K., Puckett, M. K., Chen, R., Lowther, W. T., and Howlett, A. C. (2020) Cannabinoid receptor interacting protein 1a (CRIP1a) in health and disease. *Biomolecules* **10**, 1609
6. Stadel, R., Ahn, K. H., and Kendall, D. A. (2011) The cannabinoid type-1 receptor carboxyl-terminus, more than just a tail. *J. Neurochem.* **117**, 1–18
7. Nie, J., and Lewis, D. L. (2001) The proximal and distal C-terminal tail domains of the CB_1 cannabinoid receptor mediate G protein coupling. *Neuroscience* **107**, 161–167
8. Niehaus, J. L., Liu, Y., Wallis, K. T., Egertova, M., Bhartur, S. G., Mukhopadhyay, S., Shi, S., He, H., Selley, D. E., Howlett, A. C., Elphick, M. R., and Lewis, D. L. (2007) CB_1 cannabinoid receptor activity is

modulated by the cannabinoid receptor interacting protein CRIP 1a. *Mol. Pharmacol.* **72**, 1557–1566
9. Smith, T. H., Blume, L. C., Straiker, A., Cox, J. O., David, B. G., McVoy, J. R., Sayers, K. W., Poklis, J. L., Abdullah, R. A., Egertova, M., Chen, C. K., Mackie, K., Elphick, M. R., Howlett, A. C., and Selley, D. E. (2015) Cannabinoid receptor-interacting protein 1a modulates CB_1 receptor signaling and regulation. *Mol. Pharmacol.* **87**, 747–765
10. Blume, L. C., Eldeeb, K., Bass, C. E., Selley, D. E., and Howlett, A. C. (2015) Cannabinoid receptor interacting protein (CRIP1a) attenuates CB_1R signaling in neuronal cells. *Cell. Signal.* **27**, 716–726
11. Booth, W. T., Walker, N. B., Lowther, W. T., and Howlett, A. C. (2019) Cannabinoid receptor interacting protein 1a (CRIP1a): Function and structure. *Molecules* **24**, 3672
12. Chun, E., Thompson, A. A., Liu, W., Roth, C. B., Griffith, M. T., Katritch, V., Kunken, J., Xu, F., Cherezov, V., Hanson, M. A., and Stevens, R. C. (2012) Fusion partner toolchest for the stabilization and crystallization of G protein-coupled receptors. *Structure* **20**, 967–976
13. Anand, N. N., Stephen, E. R., and Narang, S. A. (1988) Mutation of active site residues in synthetic T4-lysozyme gene and their effect on lytic activity. *Biochem. Biophys. Res. Commun.* **153**, 862–868
14. Sun, D. P., Alber, T., Bell, J. A., Weaver, L. H., and Matthews, B. W. (1987) Use of site-directed mutagenesis to obtain isomorphous heavy-atom derivatives for protein crystallography: Cysteine-containing mutants of phage T4 lysozyme. *Protein Eng.* **1**, 115–123
15. Adams, P. D., Afonine, P. V., Bunkoczi, G., Chen, V. B., Echols, N., Headd, J. J., Hung, L. W., Jain, S., Kapral, G. J., Grosse Kunstleve, R. W., McCoy, A. J., Moriarty, N. W., Oeffner, R. D., Read, R. J., Richardson, D. C., *et al.* (2011) The Phenix software for automated determination of macromolecular structures. *Methods* **55**, 94–106
16. Ahmed, M. H., Kellogg, G. E., Selley, D. E., Safo, M. K., and Zhang, Y. (2014) Predicting the molecular interactions of CRIP1a-cannabinoid 1 receptor with integrated molecular modeling approaches. *Bioorg. Med. Chem. Lett.* **24**, 1158–1165
17. Singh, P., Ganjiwale, A., Howlett, A. C., and Cowsik, S. M. (2017) In silico interaction analysis of cannabinoid receptor interacting protein 1b (CRIP1b) - CB_1 cannabinoid receptor. *J. Mol. Graph. Model.* **77**, 311–321
18. DerMardirossian, C., and Bokoch, G. M. (2005) GDIs: Central regulatory molecules in Rho GTPase activation. *Trends Cell Biol.* **15**, 356–363
19. Dovas, A., and Couchman, J. R. (2005) RhoGDI: Multiple functions in the regulation of Rho family GTPase activities. *Biochem. J.* **390**, 1–9
20. Dransart, E., Olofsson, B., and Cherfils, J. (2005) RhoGDIs revisited: Novel roles in Rho regulation. *Traffic* **6**, 957–966
21. Deutsch, D. G. (2016) A personal retrospective: Elevating anandamide (AEA) by targeting fatty acid amide hydrolase (FAAH) and the fatty acid binding proteins (FABPs). *Front. Pharmacol.* **7**, 370
22. Bukiya, A. N., and Dopico, A. M. (2019) Cannabinoid interactions with proteins: Insights from structural studies. *Adv. Exp. Med. Biol.* **1162**, 39–50
23. Kaczocha, M., Glaser, S. T., and Deutsch, D. G. (2009) Identification of intracellular carriers for the endocannabinoid anandamide. *Proc. Natl. Acad. Sci. U. S. A.* **106**, 6375–6380
24. Sanson, B., Wang, T., Sun, J., Wang, L., Kaczocha, M., Ojima, I., Deutsch, D., and Li, H. (2014) Crystallographic study of FABP5 as an intracellular endocannabinoid transporter. *Acta Crystallogr. D Biol. Crystallogr.* **70**, 290–298
25. Elmes, M. W., Kaczocha, M., Berger, W. T., Leung, K., Ralph, B. P., Wang, L., Sweeney, J. M., Miyauchi, J. T., Tsirka, S. E., Ojima, I., and Deutsch, D. G. (2015) Fatty acid-binding proteins (FABPs) are intracellular carriers for Delta9-tetrahydrocannabinol (THC) and cannabidiol (CBD). *J. Biol. Chem.* **290**, 8711–8721
26. Silvaroli, J. A., Widjaja-Adhi, M. A. K., Trischman, T., Chelstowska, S., Horwitz, S., Banerjee, S., Kiser, P. D., Blaner, W. S., and Golczak, M. (2019) Abnormal cannabidiol modulates vitamin A metabolism by acting as a competitive inhibitor of CRBP1. *ACS Chem. Biol.* **14**, 434–448
27. Holm, L. (2020) Using Dali for protein structure comparison. *Methods Mol. Biol.* **2112**, 29–42
28. Stephen, L. A., and Ismail, S. (2016) Shuttling and sorting lipid-modified cargo into the cilia. *Biochem. Soc. Trans.* **44**, 1273–1280
29. Chandra, A., Grecco, H. E., Pisupati, V., Perera, D., Cassidy, L., Skoulidis, F., Ismail, S. A., Hedberg, C., Hanzal-Bayer, M., Venkitaraman, A. R., Wittinghofer, A., and Bastiaens, P. I. (2011) The GDI-like solubilizing factor PDEdelta sustains the spatial organization and signalling of Ras family proteins. *Nat. Cell Biol.* **14**, 148–158
30. Fansa, E. K., Kosling, S. K., Zent, E., Wittinghofer, A., and Ismail, S. (2016) PDE6delta-mediated sorting of INPP5E into the cilium is determined by cargo-carrier affinity. *Nat. Commun.* **7**, 11366
31. Papke, B., Murarka, S., Vogel, H. A., Martin-Gago, P., Kovacevic, M., Truxius, D. C., Fansa, E. K., Ismail, S., Zimmermann, G., Heinelt, K., Schultz-Fademrecht, C., Al Saabi, A., Baumann, M., Nussbaumer, P., Wittinghofer, A., *et al.* (2016) Identification of pyrazolopyridazinones as PDEdelta inhibitors. *Nat. Commun.* **7**, 11360
32. Jaiswal, M., Fansa, E. K., Kosling, S. K., Mejuch, T., Waldmann, H., and Wittinghofer, A. (2016) Novel biochemical and structural insights into the interaction of myristoylated cargo with Unc119 protein and their release by Arl2/3. *J. Biol. Chem.* **291**, 20766–20778
33. Mattheus, T., Kukla, K., Zimmermann, T., Tenzer, S., and Lutz, B. (2016) Cell type-specific tandem affinity purification of the mouse hippocampal CB_1 receptor-associated proteome. *J. Proteome Res.* **15**, 3585–3601
34. Njoo, C., Agarwal, N., Lutz, B., and Kuner, R. (2015) The cannabinoid receptor CB_1 interacts with the WAVE1 complex and plays a role in actin dynamics and structural plasticity in neurons. *PLoS Biol.* **13**, e1002286
35. Ismail, S. A., Chen, Y. X., Rusinova, A., Chandra, A., Bierbaum, M., Gremer, L., Triola, G., Waldmann, H., Bastiaens, P. I., and Wittinghofer, A. (2011) Arl2-GTP and Arl3-GTP regulate a GDI-like transport system for farnesylated cargo. *Nat. Chem. Biol.* **7**, 942–949
36. Blume, L. C., Patten, T., Eldeeb, K., Leone-Kabler, S., Ilyasov, A. A., Keegan, B. M., O'Neal, J. E., Bass, C. E., Hantgan, R. R., Lowther, W. T., Selley, D. E., and Howlett, A. L. (2017) Cannabinoid receptor interacting protein 1a competition with beta-arrestin for CB_1 receptor binding sites. *Mol. Pharmacol.* **91**, 75–86
37. Mukhopadhyay, S., and Howlett, A. C. (2001) CB_1 receptor-G protein association. Subtype selectivity is determined by distinct intracellular domains. *Eur. J. Biochem.* **268**, 499–505
38. Hua, T., Vemuri, K., Nikas, S. P., Laprairie, R. B., Wu, Y., Qu, L., Pu, M., Korde, A., Jiang, S., Ho, J. H., Han, G. W., Ding, K., Li, X., Liu, H., Hanson, M. A., *et al.* (2017) Crystal structures of agonist-bound human cannabinoid receptor CB_1. *Nature* **547**, 468–471
39. Hua, T., Vemuri, K., Pu, M., Qu, L., Han, G. W., Wu, Y., Zhao, S., Shui, W., Li, S., Korde, A., Laprairie, R. B., Stahl, E. L., Ho, J. H., Zvonok, N., Zhou, H., *et al.* (2016) Crystal structure of the human cannabinoid receptor CB_1. *Cell* **167**, 750–762
40. Krishna Kumar, K., Shalev-Benami, M., Robertson, M. J., Hu, H., Banister, S. D., Hollingsworth, S. A., Latorraca, N. R., Kato, H. E., Hilger, D., Maeda, S., Weis, W. I., Farrens, D. L., Dror, R. O., Malhotra, S. V., Kobilka, B. K., *et al.* (2019) Structure of a signaling cannabinoid receptor 1-G protein complex. *Cell* **176**, 448–458
41. Hua, T., Li, X., Wu, L., Iliopoulos-Tsoutsouvas, C., Wang, Y., Wu, M., Shen, L., Brust, C. A., Nikas, S. P., Song, F., Song, X., Yuan, S., Sun, Q., Wu, Y., Jiang, S., *et al.* (2020) Activation and signaling mechanism revealed by cannabinoid receptor-Gi complex structures. *Cell* **180**, 655–665
42. Mascia, F., Klotz, L., Lerch, J., Ahmed, M. H., Zhang, Y., and Enz, R. (2017) CRIP1a inhibits endocytosis of G-protein coupled receptors activated by endocannabinoids and glutamate by a common molecular mechanism. *J. Neurochem.* **141**, 577–591
43. Chu, R., Takei, J., Knowlton, J. R., Andrykovitch, M., Pei, W., Kajava, A. V., Steinbach, P. J., Ji, X., and Bai, Y. (2002) Redesign of a four-helix bundle protein by phage display coupled with proteolysis and structural characterization by NMR and X-ray crystallography. *J. Mol. Biol.* **323**, 253–262

44. Mooers, B. H., Tronrud, D. E., and Matthews, B. W. (2009) Evaluation at atomic resolution of the role of strain in destabilizing the temperature-sensitive T4 lysozyme mutant Arg 96–> His. *Protein Sci.* **18**, 863–870
45. Emsley, P., Lohkamp, B., Scott, W. G., and Cowtan, K. (2010) Features and development of Coot. *Acta Crystallogr. D Biol. Crystallogr.* **66**, 486–501
46. Chen, V. B., Arendall, W. B., 3rd, Headd, J. J., Keedy, D. A., Immormino, R. M., Kapral, G. J., Murray, L. W., Richardson, J. S., and Richardson, D. C. (2010) MolProbity: All-atom structure validation for macromolecular crystallography. *Acta Crystallogr. D Biol. Crystallogr.* **66**, 12–21
47. Liu, J., Gao, J., Li, F., Ma, R., Wei, Q., Wang, A., Wu, J., and Ruan, K. (2017) NMR characterization of weak interactions between RhoGDI2 and fragment screening hits. *Biochim. Biophys. Acta Gen. Subj.* **1861**, 3061–3070

William T. Booth is an Assistant Professor of Chemistry in the Department of Natural Sciences and Mathematics at Johnson C. Smith University. He studies a variety of proteins using biochemical and structural biology approaches. In the present report, he determined the first structure of the cannabinoid receptor interacting protein 1a and identified a novel mechanism for the regulation of this G protein–coupled receptor. His current interests include training STEM students by exploring proteins involved in nicotinamide adenine dinucleotide biosynthesis.